Numerical Methods in Civil Engineering

Static and Dynamic Safety Evaluation of A Heightened Arch Dam Including Massed Foundation Effects

H. Mirzabozorg*, M. Ghaemian**, and S.M. Aghajanzadeh***

ARTICLE INFO

Article history:
Received:
April 2020.
Revised:
June 2020.
Accepted:
June 2020.

Keywords:
DEZ dam; Fluid-Structure Interaction, Heightening Plan; Massed Foundation, Seismic safety evaluation

Abstract:

DEZ dam is a double curvature arch dam built between 1959 and 1963. After more than 50 years of operation, the reservoir's storage capacity was reduced due to sedimentation, threatening its useful life and power intake. Several solutions were examined, and heightening the dam body was chosen as the most economical solution. Consequently, the seismic safety of the heightened structure was seen as indispensable. This study investigates the seismic safety of DEZ dam, considering the effects of heightening the dam body. Static loads and two levels of OBE and MCE earthquakes are applied to the finite element model of the dam-massed foundation-reservoir system. In static loadings, local stress concentration occurs in the heightened dam. Additionally, under the OBE earthquake, some limited damage is predicted, which is not problematic for dam safety. Finally, Under MCE records, some cracked regions are developed. Still, the model does not show general instability, and so, the cracked areas do not lead to the release of the reservoir.

1. Introduction

Concrete dams as infrastructures are built to manage and store water used in irrigation, power generation, and flood control. After years of operation, these expensive structures may fail to achieve their predefined goals. Accordingly, redeveloping and modifying these costly structures is crucial as probable failure to achieve the predefined goals may cause economic, environmental, and several other drawbacks. Among different solutions of reforming, heightening the dam body is one of the options. Examples of heightening can be found in some projects. Mauvision double curvature arch dam was built to a height of 237 m during 1951-1957 and then was raised by 13m during 1989-1991. With 237 m height, the reservoir was filled in late summer, and autumn flow storage was not possible. Solving the reservoir capacity shortages, the dam body was increased to 250m during 1989-1991[1]. In another project, the height of the Mangla dam was raised about 10m to restore storage capacity, which was lost due to the sedimentation problem. The project was completed in October 2011 [2]. Another dam whose height was increased is the San Vicente dam. The roller-compacted concrete San Vicente dam height was raised by 17m to expand its reservoir capacity and water supply [3].

DEZ double curvature arch dam, which is the main issue of the current study, is another dam facing a storage capacity problem due to sedimentation. Sedimentation is a common problem that can disrupt a dam's optimal performance by shortening the useful life and reservoir capacity. The DEZ dam reservoir's initial storage capacity was 3315mcm. After more than 50 years of operation, the reservoir volume decreased to 2600mcm since sedimentation height reached near power intake level around 30m above the irrigation outlets [4]. As another example, the Sefid-Rud reservoir located north of Iran (built-in 1962) lost 30% of its capacity in 1980 due to sedimentation [6].

In recent years, several studies have investigated sedimentation problems. Graf et al. investigated the sustainability of Missouri and Colorado River basins considering sedimentation measurement. They concluded that the reservoir storage capacity's sedimentation and loss rate are highly variable in time and space [7]. Issa studied Mosul dam Reservoir and found that sediment deposition

**Corresponding Author: Associate Professor, Department of Civil Engineering, K. N. Toosi University of Technology, Tehran, Iran. Email: mirzabozorg@kntu.ac.ir*
*** Associate Professor, Department of Civil Engineering, Sharif University of Technology, Tehran, Iran*
****Ph.D., Department of Civil Engineering, K. N. Toosi University of Technology, Tehran, Iran.*

reduced 14.73% of the reservoir's total storage capacity [8]. Kondolf et al. studied issues of sediments trapped in dam reservoirs. They recommended that a full range of sediment passage options should be considered for dams not yet built, while other options to improve sediment management should be applied to existing dams [9]. Tang et al. studied transportation and sedimentation of particulate phosphorus in the Three Gorges Reservoir [10]. Huang et al. investigated the Three Gorges Reservoir, and they concluded that the incoming sediment load and the accumulated volume of sediment deposition are smaller than expected. Still, the possible increase in sediment risks should be considered [11]. Guertault and Fox studied the effects of field data availability and resolution on reservoir sedimentation predictions considering Fort Cobb Reservoir [12]. Tadesse and Dai investigated sediment load reaching the Kola Dam Reservoir in Ethiopia on the Awash River basin using the loose integration of the Soil and Water Assessment Tool model and Hydrological Engineering Center-River Analysis System [13].

Alongside solving the sedimentation problem in DEZ, Boroujeni investigated different solutions for sediments accumulated in the DEZ reservoir: watershed management, sediment routing, sediment flushing, and sediment removal and disposal, and dam heightening [4]. Among the solutions mentioned, flushing sediments through the dam irrigation outlets was first carried out in 1994 and then repeated annually [14]. But sedimentation released by flushing was mostly cohesive, initiating environmental issues downstream, while water stored in the reservoir was lost and other conceivable problems were likely to occur [4]. Among different solutions, in 2012, the decision was made to increase the dam body's height, but the heightening was restricted to 10m due to environmental limitations and some related surrounding restrictions like a nationwide railroad in the reservoir's vicinity. This solution would lead to an 800mcm increase in reservoir capacity [4]. Thereupon, investigating the safe performance of the initial dam and heightening dam is essential.

Different studies evaluated the safe performance of concrete dams. Ghorbani et al. studied seismic performance of double curvature Morrow Point concrete dam, considering non-linear mass concrete behavior [15]. Ghaemian et al. studied the effects of foundation mass and earthquake input mechanism on a concrete gravity dam's seismic performance considering two different free-field boundary conditions and the domain reduction method. Based on their results, the effects of massed foundation on the dam responses are notable and massless foundation overestimates the dam response [16]. Mostafaei et al. evaluated the accuracy of pseudo-static and dynamic methods for arch dams' abutment stability [17]. In another study, Mostafaei et al compared the obtained time history of sliding safety factors to the quasi-static results for the Luzzone dam [18]. Chen et al. investigated the potential failure modes of a typical non-overflow dam section of Jin'anqiao roller-compacted concrete gravity dam utilizing the incremental dynamic analysis (IDA) method. Based on their results, the regions of the dam body for strengthening were verified [19]. Lin et al. investigated the Xiluodo super-high arch dam's horizontal cracking and proposed a crack repair design based on the fracture toughness method [20].

This study investigates the safe performance of the initial and heightened structure of the DEZ dam. For dynamic loading, two levels of OBE and MCE excitations are applied. Initial dam dynamic analysis is performed under MCE excitation, while the heightened structure dynamic analysis is conducted under both MCE and OBE excitations. The reservoir is modeled to be compressible, and the foundation is assumed to be massed. Effects of vertical joints are considered, and both non-linear and linear behaviors of mass concrete are investigated. The numerical model of material nonlinearity considers the effects of concrete cracking and crushing. Initial and heightened structures are analyzed separately.

2. DEZ Dam

The DEZ double curvature arch dam, constructed between 1959 and 1963, with an initial height of 203m (from the bottom of the plug) is located in the Southwest of Iran. Its main object was to supply water for irrigation, power generation, and flood control [21]. The dam has a peripheral joint separating the dam body from a concrete saddle structure called PULVINO. Additionally, the overall joint was provided between the dam body and PULVINO, commonly called peripheral joint. The downstream view of the dam body with saddle structure (PULVINO) is shown in Fig. **1** [22], and the general characteristics of the dam are presented in Table 1 [23].

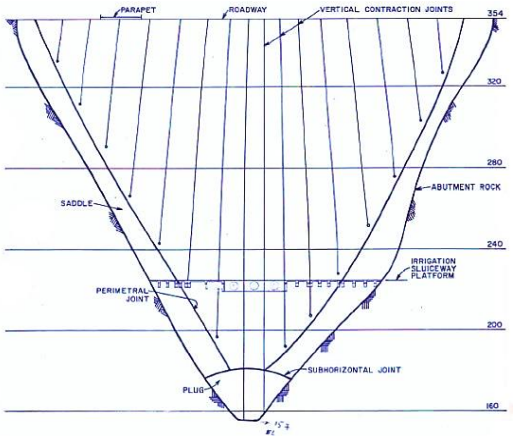

Fig. 1: Downstream view of the dam body

Table 1: General characteristics of the DEZ arch dam [23]

Maximum height above the foundation	203.5m
Crest length	240m
Crest thickness	4.5m
Base thickness at body/PULVINO	21m/28m
Concrete volume (dam only)	328000cm
Concrete volume (dam and PULVINO)	142000cm
Total concrete volume	470000cm
Maximum water level	352masl
Normal operational level	350masl
Minimum operational level	290masl
Full reservoir capacity	3350mcm

2.1 Heightening Plan of the Dam

As mentioned previously, a plan for heightening the existing dam was proposed, in which the dam crest was raised by 7.65m continuing through the upstream and downstream faces smoothly as shown in Fig. **2**. This heightening led to an increased normal water level from 352masl to 360masl, which makes an 800mcm increase in the reservoir's useful volume. It is worth noting that a gallery with the width and height of 1m and 2m was installed along the heightened structure, leading to a decrease in the weight and inertia force.

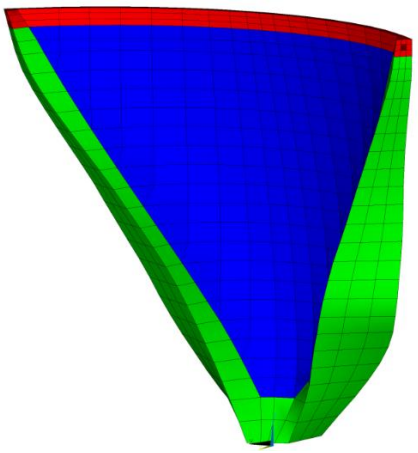

Fig. 2: Existing dam, PULVINO and heightening structure

3. Material Model

This section clarifies the non-linear behavior of concrete in tension and compression and presents the joint nonlinearity properties. Mechanical properties of concrete, joints, and sedimentation are similar to those used by Hariri-Ardebili and Mirzabozorg [24].

3.1 Mechanical Properties of Concrete

Cracking at each Gaussian point in three orthogonal directions is allowed, and if cracking occurs at a Gaussian point, the crack is modeled directly with modifying material properties. The failure of concrete is categorized into four domains, considering cracking and crushing. Table 2 shows the four domains considered for concrete failure:

Table 2: Four domains for concrete failure

Domain	Principal Stress	Stress State
1	$0 \geq \sigma_1 \geq \sigma_2 \geq \sigma_3$	(compression - compression - compression)
2	$\sigma_1 \geq 0 \geq \sigma_2 \geq \sigma_3$	(tensile - compression - compression)
3	$\sigma_1 \geq \sigma_2 \geq 0 \geq \sigma_3$	(tensile - tensile - compression)
4	$\sigma_1 \geq \sigma_2 \geq \sigma_3 \geq 0$	(tensile - tensile - tensile)

Concrete material is initially isotropic, and the relationship of the stress and strain vectors at the pre-softening phase is given as:

$$[D^e] = \frac{E}{(1+\upsilon)(1-2\upsilon)} \begin{bmatrix} (1-\upsilon) & \upsilon & \upsilon & 0 & 0 & 0 \\ \upsilon & (1-\upsilon) & \upsilon & 0 & 0 & 0 \\ \upsilon & \upsilon & (1-\upsilon) & 0 & 0 & 0 \\ 0 & 0 & 0 & \frac{1-2\upsilon}{2} & 0 & 0 \\ 0 & 0 & 0 & 0 & \frac{1-2\upsilon}{2} & 0 \\ 0 & 0 & 0 & 0 & 0 & \frac{1-2\upsilon}{2} \end{bmatrix} \quad (1)$$

where E is the elastic modulus matrix, and υ is Poisson's ratio. The Five-parameter Willam-Warnke model predicts the occurrence of a failure in mass concrete [25]. So, the criterion for the concrete failure due to a multi-axial stress state is expressed in the form as:

$$\frac{\Omega}{f_c} - \gamma \geq 0 \quad (2)$$

where, Ω is a function of stress state; γ is the failure surface defined in terms of principal stresses and the five input parameters, which are described in table 3.

Table 3: Concrete material table

Label	Description
f_t	Ultimate uniaxial tensile strength
f_c	Ultimate uniaxial compressive strength
f_{cb}	Ultimate biaxial compressive strength
σ_h^a	Ambient hydrostatic stress state
f_1	Ultimate compressive strength for a state of biaxial compression superimposed on hydrostatic state
f_2	Ultimate compressive strength for a state of uniaxial compression superimposed on hydrostatic state

If equation (2) is fulfilled, cracking or crushing of concrete occurs. In that case, whenever one of the principal stresses in concrete is tensile with a value more than the relevant strength, the crack occurs. Also, when all principal stresses are compressive, crushing occurs. The failure surface can be specified with two parameters f_c and f_t. The other parameters can be calculated in the Willam-Warnke model by default as follows [25]:

$$f_{cb} = 1.2 f_c \tag{3}$$

$$f_1 = 1.45 f_c \tag{4}$$

$$f_2 = 1.725 f_c \tag{5}$$

This model allows cracking in three orthogonal directions at each Gaussian point. The presence of crack at a Gaussian point and in a special direction is reflected in the stiffness matrix as following [24]:

$$[D_c^{ck}] = \frac{E}{1+\nu}\begin{bmatrix} \frac{R^t(1+\nu)}{E} & 0 & 0 & 0 & 0 & 0 \\ 0 & \frac{1}{1-\nu} & \frac{\nu}{1-\nu} & 0 & 0 & 0 \\ 0 & \frac{\nu}{1-\nu} & \frac{1}{1-\nu} & 0 & 0 & 0 \\ 0 & 0 & 0 & \frac{\beta_t}{2} & 0 & 0 \\ 0 & 0 & 0 & 0 & \frac{1}{2} & 0 \\ 0 & 0 & 0 & 0 & 0 & \frac{\beta_t}{2} \end{bmatrix} \tag{6}$$

Superscript *ck* states that the strain-stress relationship is in the coordinate system parallel to the direction of principle stresses. Axis X_{ck} is orthogonal to crack plane, and the value of parameter R^t in the equation (6) is secant stiffness in tensile condition, which is shown in Fig. 3:

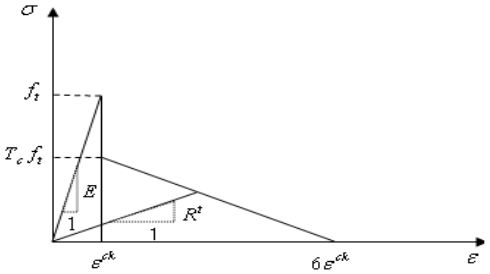

Fig. 3: Strain-stress curve of concrete mass in tension [24]

In Fig. 3, T_c is the reduction coefficient of tensile stress. If a crack is closed, all compressive stresses orthogonal to the crack plane can be transmitted, and only a shear transfer coefficient is applied to the matrix. The value of this parameter in the present study is equal to 0.9 [24], so for closed crack, the strain-stress element matrix is calculated as follows:

$$[D_c^{ck}] = \frac{E}{(1+\nu)(1-2\nu)}\begin{bmatrix} (1-\nu) & \nu & \nu & 0 & 0 & 0 \\ \nu & (1-\nu) & \nu & 0 & 0 & 0 \\ \nu & \nu & (1-\nu) & 0 & 0 & 0 \\ 0 & 0 & 0 & \frac{\beta_t(1-2\nu)}{2} & 0 & 0 \\ 0 & 0 & 0 & 0 & \frac{1-2\nu}{2} & 0 \\ 0 & 0 & 0 & 0 & 0 & \frac{\beta_c(1-2\nu)}{2} \end{bmatrix} \tag{7}$$

In the following, if the concrete is cracked in two directions, we have:

$$[D_c^{ck}] = E\begin{bmatrix} \frac{R^t}{E} & 0 & 0 & 0 & 0 & 0 \\ 0 & \frac{R^t}{E} & 0 & 0 & 0 & 0 \\ 0 & 0 & 1 & 0 & 0 & 0 \\ 0 & 0 & 0 & \frac{\beta_t}{2(1+\nu)} & 0 & 0 \\ 0 & 0 & 0 & 0 & \frac{\beta_t}{1(1+\nu)} & 0 \\ 0 & 0 & 0 & 0 & 0 & \frac{\beta_t}{2(1+\nu)} \end{bmatrix} \tag{8}$$

and if cracks are closed in two directions:

$$[D_c^{ck}] = \frac{E}{(1+\nu)(1-2\nu)}\begin{bmatrix} (1-\nu) & \nu & \nu & 0 & 0 & 0 \\ \nu & (1-\nu) & \nu & 0 & 0 & 0 \\ \nu & \nu & (1-\nu) & 0 & 0 & 0 \\ 0 & 0 & 0 & \frac{\beta_c(1-2\nu)}{2} & 0 & 0 \\ 0 & 0 & 0 & 0 & \frac{(1-2\nu)}{2} & 0 \\ 0 & 0 & 0 & 0 & 0 & \frac{\beta_c(1-2\nu)}{2} \end{bmatrix} \tag{9}$$

Finally, strain stress relationship for concrete that is cracked in three directions, we have:

$$[D_c^{ck}] = E\begin{bmatrix} \frac{R^t}{E} & 0 & 0 & 0 & 0 & 0 \\ 0 & \frac{R^t}{E} & 0 & 0 & 0 & 0 \\ 0 & 0 & 1 & 0 & 0 & 0 \\ 0 & 0 & 0 & \frac{\beta_t}{2(1+\nu)} & 0 & 0 \\ 0 & 0 & 0 & 0 & \frac{\beta_t}{2(1+\nu)} & 0 \\ 0 & 0 & 0 & 0 & 0 & \frac{\beta_t}{2(1+\nu)} \end{bmatrix} \tag{10}$$

It is worth noting that the relationship between β_t and β_c is always as follows:

$$0 < \beta_t < \beta_c < 1 \tag{11}$$

In the present study, the value of the parameter β_t is taken 0.2 [24]. Finally, the cracked element matrix is transferred to the element coordinate system by transfer matrix $[T^{ck}]$:

$$[D_c] = [T^{ck}][D_c^{ck}][T^{ck}] \tag{12}$$

The above transfer matrix is a function of crack strain. It is noticed that if at a point the concrete in the uni-axial, biaxial or tri-axial case is fractured, the concrete is considered as crushed. The crushed Gaussian point is completely eliminated from the stiffness matrix, and its force is allocated to adjacent ones.

3.2 Mechanical Properties of Joints

A special contact element is used for modeling joints, which only supports compression in the normal direction and shears in the tangential direction. So, normal and tangential entities in the stiffness matrix are not coupled. Fig. **4** shows the flowchart used for calculating force in contact elements. V_n indicates the state in the normal direction to the plane of

the joint, and V_r and V_s indicate the state of the considered contact element in tangential directions. Moreover, c is the cohesion factor, and μ is the friction coefficient [24].

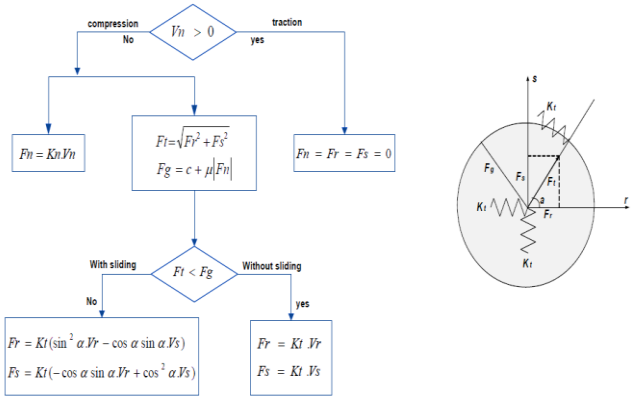

Fig. 4: Flowchart for calculating force in joints [24]

Moreover, Fig. **5** shows force-deflection relations for both normal and tangential directions. F_n, F_r, and F_s are local components of the force vector; F_g is the joint's sliding force; F_t is the shear force resultant; K_n and K_t are the normal and tangential stiffness, and α is the angle between the two components of in-plane shear. As shown, a contact element cannot endure any tensile force or stress, but when it is in compression, it can suffer compression forces according to its normal stiffness coefficient and shear forces according to its tangential stiffness coefficient [24].

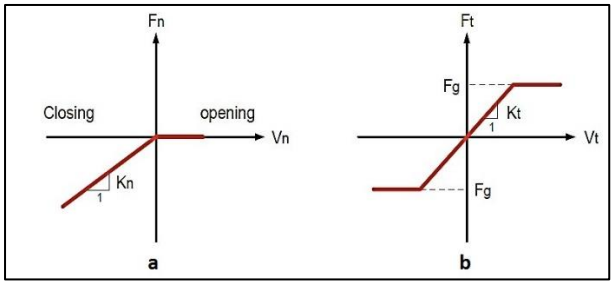

Fig. 5: Force-deflection relations for joint: (a) normal opening (left); (b) tangential movement (right) [24]

Element stiffness matrix in three different cases is considered as follows:

1- Joint is closed numerically, and there is no sliding:

$$[K]=\begin{bmatrix} K_n & 0 & 0 & -K_n & 0 & 0 \\ 0 & K_t & 0 & 0 & -K_t & 0 \\ 0 & 0 & K_t & 0 & 0 & -K_t \\ -K_n & 0 & 0 & K_n & 0 & 0 \\ 0 & -K_t & 0 & 0 & K_t & 0 \\ 0 & 0 & -K_t & 0 & 0 & K_t \end{bmatrix} \quad (13)$$

2- Joint is closed numerically, but the two adjacent nodes are sliding towards each other:

$$[K]=\begin{bmatrix} K_n & 0 & 0 & -K_n & 0 & 0 \\ 0 & 0 & 0 & 0 & 0 & 0 \\ 0 & 0 & 0 & 0 & 0 & 0 \\ -K_n & 0 & 0 & K_n & 0 & 0 \\ 0 & 0 & 0 & 0 & 0 & 0 \\ 0 & 0 & 0 & 0 & 0 & 0 \end{bmatrix} \quad (14)$$

3- Joint is opened numerically, and there is no contact between adjacent nodes:

$$[K]=[0]_{6\times 6} \quad (15)$$

4. Numerical Model

4.1 Parameters Calibration and Mechanical properties

Precise and reliable analysis of a dam is possible if all the material parameters are derived via a calibration process conducted by instruments installed inside the dam body. Hariri-Ardebili et al. reported the static and thermal calibration process of the DEZ dam [24]. Transient thermal analysis based on thermometers records installed in the central block was carried out, and thermal distribution, dam self-weight, hydrostatic pressure, and silt load were considered for static calibration. Temperature distribution along the reservoir depth was calculated by the Bofang approach, and ambient temperature was obtained by a thermometer placed on the dam crest. A transient heat transfer analysis was performed to calculate temperature distribution within the dam body, and results were compared with thermometers installed in central block [24].

In the static calibration procedure applied on the dam body displacement, the micro-geodetic observations series numbered 9th, 10th, 11th, and 15th were selected for the numerical model's sensitive analysis and calibration process. Moreover, based on sensitivity analysis, the K_n and K_s of the vertical joints were 210GPa/m and 16.8GPa/m, respectively. Table 4 shows a summary of the calibration results [24]. Based on the calibration results, the material's mechanical properties are chosen (based on table 4). So, for the mass concrete, modulus of elasticity, Poisson's ratio, and the unit weight are chosen 40GPa, 0.2, 24.0kN/m^3, respectively. Reference temperature and thermal expansion coefficient are selected 23°C and 6×10^{-6}/°C, respectively.

Table 4: Mechanical properties of mass concrete and foundation of DEZ dam [24]

Mass Concrete	Density	2400 kg/m^3
	Modulus of Elasticity	40GPa
	Poisson's ratio	0.2
	Thermal Expansion Coefficient	6×10^{-6} /°C
	Grouting Temperature	23°C

Foundation Rock	Deformation Modulus (Saturated/Dry Region)	13 GPa, 15GPa
	Unit Weight (Saturated/Dry Region)	25 kN/m^3, 24 kN/m^3
	Poisson's ratio (Saturated/Dry Region)	0.25

The true compressive strength of concrete is assumed as 35MPa. Raphael equation is used to calculate the tensile strength of concrete as follows:

$$f_t' = 0.32 f_c'^{\frac{2}{3}} = 3.4\ Mpa \quad (16)$$

Table 5 shows the values of used strength parameters in the present study in static and dynamic conditions.

Table 5: Values of strength parameters in the present study in static and dynamic conditions [24]

Parameter	Description	Static	Dynamic
E (GPa)	Modulus of elasticity	40	46
f_c(MPa)	Compressive strength of concrete	35	40
f_t (MPa)	Uniaxial tensile strength	3.40	5.10
T_c	Reduction factor of tensile stress	0.6	0.6

Figures 6 and 7 show the compressive stress-strain curvatures of concrete in static and dynamic conditions.

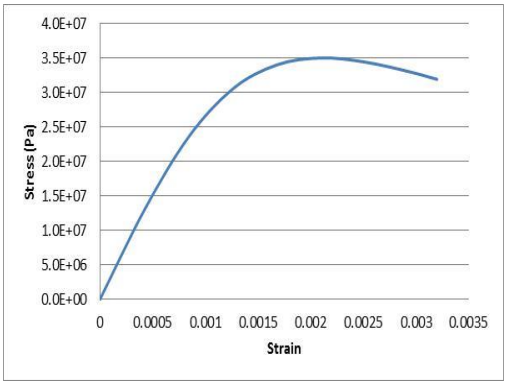

Fig. 6: Compressive stress-strain curve of concrete in static condition

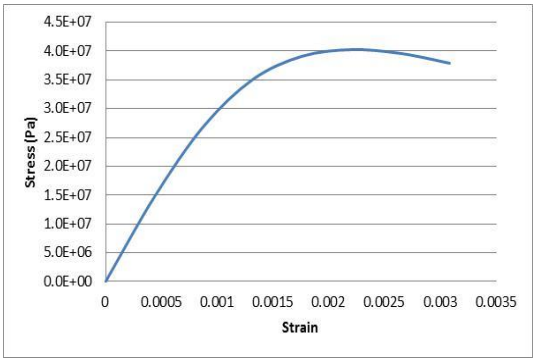

Fig. 7: Compressive stress-strain curve of concrete in dynamic condition

In the reservoir medium, the sediment level is 270masl, based on the last hydrography performed on the reservoir [4]. Submerged sediment density is assumed to be 1360kg/m^3. Pressure wave velocity and mass density within the reservoir medium are taken as 1438m/s, and 1000kg/m^3, respectively, and the wave reflection coefficient is taken as 0.8 at the reservoir bottom and sides [26].

4.2 Finite Element Model

ANSYS 11.0 software provides the finite element models (FEM). FiguresFig**. 8** andFig**. 9** show the FEM of the dam body, foundation rock, and reservoir medium. The number of elements for modeling the dam body and PULVINO is 792, and for modeling the heightening structure, surrounding foundation, and reservoir, 152, 3770, and 4530 elements are used, respectively. Also, 956 contact elements are used for modeling contraction and peripheral joints (Fig. **10**).

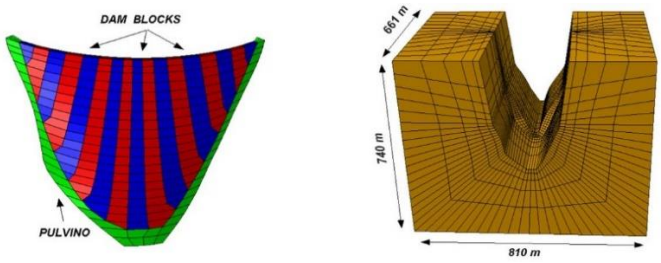

Fig. 8: Finite element model of the dam- foundation system

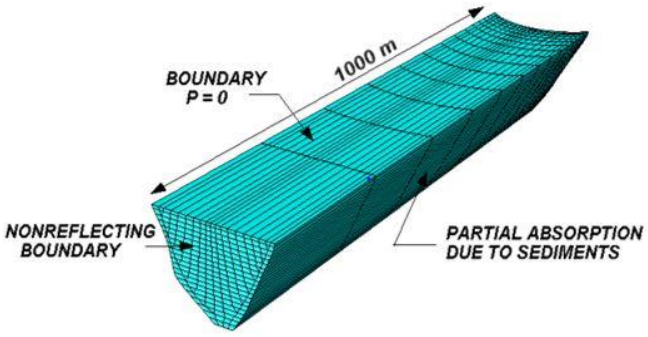

Fig. 9: FEM of the reservoir and its condition boundaries

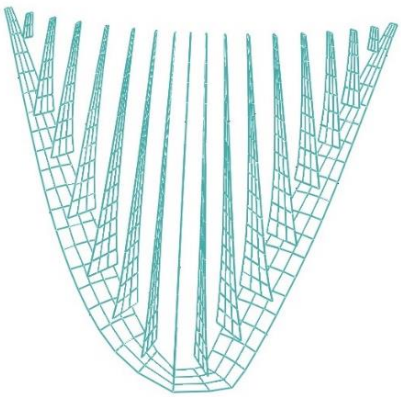

Fig. 10: Location of contraction and peripheral joints

Foundation rock was modeled concerning the topography of the site. The height, width, and length are modeled over twice the dam body's height in all directions and up to the surface of the rock in upward parts. The concrete dam body, its saddle, and foundation are modeled via eight-node solid elements. The Lysmer viscous boundary is applied to the far end nodes of the foundation medium for absorbing the outgoing waves [27].

The reservoir's length is considered over 1000m, which is about five times the dam body's height. Water is modeled using eight-node fluid elements having three translation DOFs and one pressure DOF in each node. The pressure is assumed to be zero at the free surface, and boundary conditions on the far end boundary are applied for complete absorption of hydrodynamic waves. Finally, Fig. **11** presents the heightened structure as well as its surrounding foundation

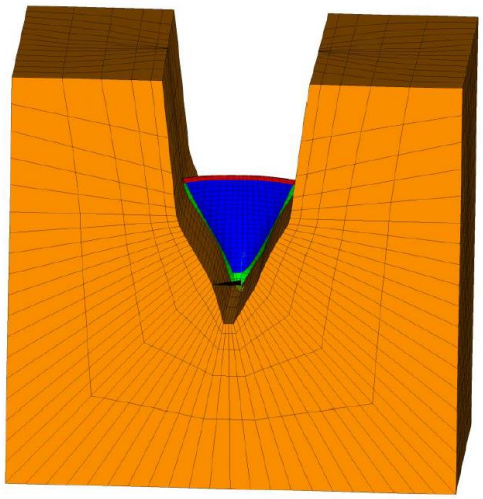

Fig. 11: Finite element model of the heightened dam

4.3 Finite Element Model

In this study, two different static load combinations are considered:

1- First Loading combination: Dead load (weight of the structure) taking into account construction stages+ hydrostatic load at normal water level (NWL) having the impounding stages+ sediment load+ thermal loading in summer conditions. In this loading combination, normal water level (NWL) is taken as 352asl and 360asl for the existing and heightened dam, respectively.

2- Second loading combination: Dead load (weight of the structure) including construction stages + hydrostatic load at minimum water level (MWL) modeling the impounding steps + sediment load+ thermal loading in winter conditions. The minimum water level is 290asl for the existing and heightened dam.

It is worth noting that, firstly, winter conditions for the existing dam are provided for modeling the construction plan. After concreting the new structure, summer or winter conditions of the heightened dam are applied. This means that the new structure must be poured in winter conditions. The heightening structure's thermal analysis is neglected due to the relatively small dimensions the dam body and its reinforcing bars. The process of staggered construction is considered to apply gravity loading. Figure 12 demonstrates this process distinguished by separate colors.

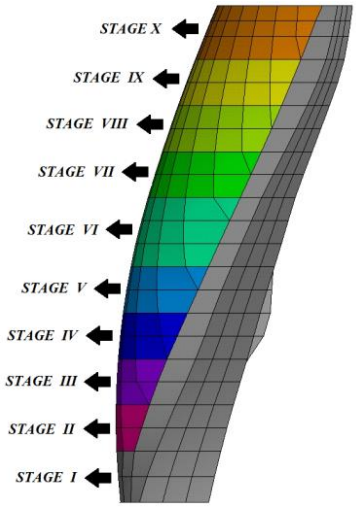

Fig. 12: 10-step construction of the dam body

4.4 Seismic Loading

Seismic evaluation of concrete arch dams should be investigated using OBE and MCE levels of excitation ground motion [28]. So, scaled NORTHRIDGE earthquake records are used for OBE excitation, while scaled MANJIL earthquake records are applied as MCE excitation. Under the OBE earthquake, the dam is expected to behave in elastic range, while in an MCE earthquake, the non-linear behavior of the dam is allowable, but its catastrophic failure should be prevented [28]. All three components are applied simultaneously through the foundation boundaries. Fig. **13** to Fig. **18** shows all three components of NORTHRIDGE and MANJIL ground motions. It is noteworthy that the applied records cover at least 95% of the amount of input seismic energy into the structure.

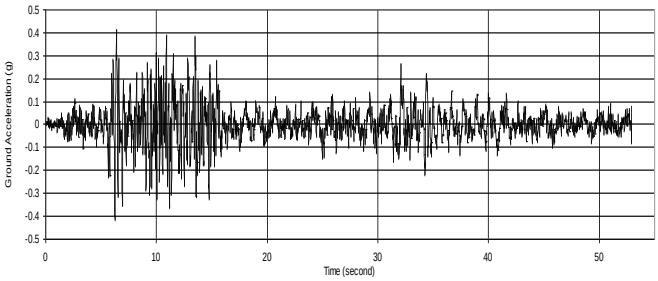

Fig. 13: Scaled accelerogram for Manjil earthquake at Abbar Station-Component L- MCE

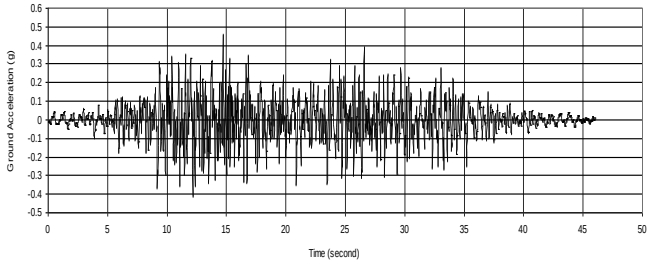

Fig. 14: Scaled accelerogram for Manjil earthquake at Abbar Station-Component T- MCE

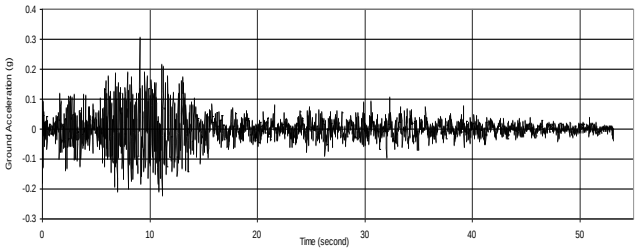

Fig. 15: Scaled accelerogram for Manjil earthquake at Abbar Station-Component V- MCE

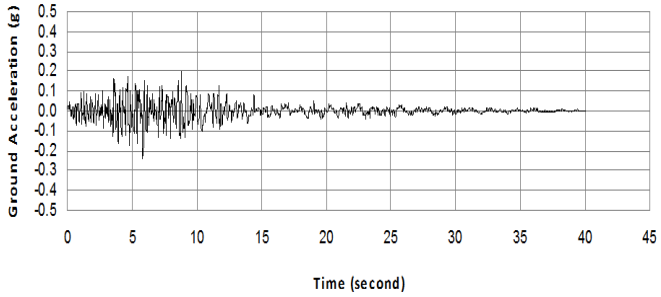

Fig. 16: Scaled accelerogarm for Northridge earthquake at 24088 PKC (Component 90, OBE)

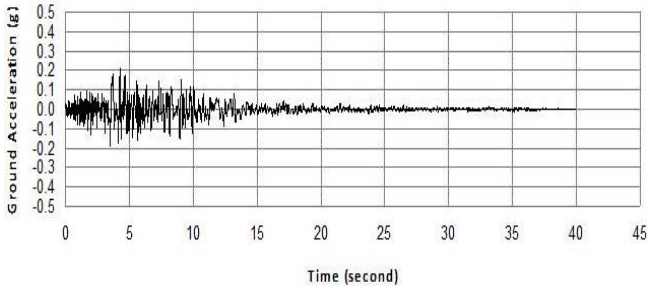

Fig. 17: Scaled accelerogarm for Northridge earthquake at 24088 PKC (Component 360, OBE)

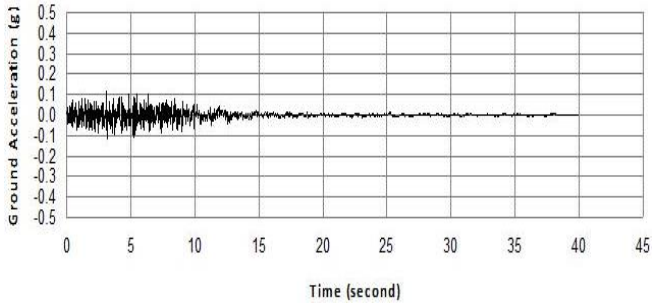

Fig. 18: Scaled accelerogram for Northridge earthquake at 24088 PKC (Component UP, OBE

One of the most important factors influencing the dynamic response is structural damping. In OBE and MCE, structural damping 5% and 10% of critical damping are considered, respectively. In the massless foundation model, the stiffness and mass proportional damping equivalent to the taken values of the critical damping based on the 2Hz and 6Hz natural frequencies of the dam-reservoir-foundation system, is applied to the system. In the massed foundation, because of violating the artificial damping due to huge mass of the surrounding foundation rock, the concept represented by Hall in 2006 is utilized, in which, based on the natural frequencies of 2Hz and 6Hz, the damping matrix [C] can be determined as [29]:

$$[c] = a_M [M] + a_K [K] \tag{17}$$

$$a_M = 2\xi\hat{\omega}\frac{2R}{1+R+2\sqrt{R}} \tag{18}$$

$$a_K = 2\xi\frac{1}{\hat{\omega}}\frac{2R}{1+R+2\sqrt{R}} \tag{19}$$

$$\hat{\omega} = 2\pi f \tag{20}$$

where, f is 2Hz, and R is 3.

5. Numerical Results

5.1 Static Analysis

Fig. **19** and Fig. **20** show maximum principal stress distribution (tensile) on the upstream and downstream faces, respectively. Static loads are applied in two different conditions of summer and winter. Comparing the maximum stress distribution at the upstream face (Fig. **19**), in lateral blocks at the crest level, tensile stresses are more significant in the heightened dam. So tensile stresses are locally larger than 3 MPa. But, at the downstream faces, tensile stresses are larger in the central blocks of the heightened dam. On both downstream and upstream faces, tensile stresses are lower than the tensile strength of mass concrete, and tensile stresses are higher in the heightened dam.

Fig. 21 and Fig. 22 show the results of minimum principal stress distributions (compressive). Investigating minimum principal stress distribution on the upstream face (Fig. 21), in the central blocks at the heightened dam's crest, compressive stresses are locally larger than 12 MPa in the summer condition. But, for both initial and heightened dam, stress distributions are almost the same. As expected, the initial dam has lower compressive stresses in winter conditions at the crest on the upstream face. On the downstream face (Fig. 22), the compressive stress distribution is more critical in the summer condition and higher for the heightened dam. In this case, high compressive stresses occur along the dam's sides, in the vicinity of the PULVINO.

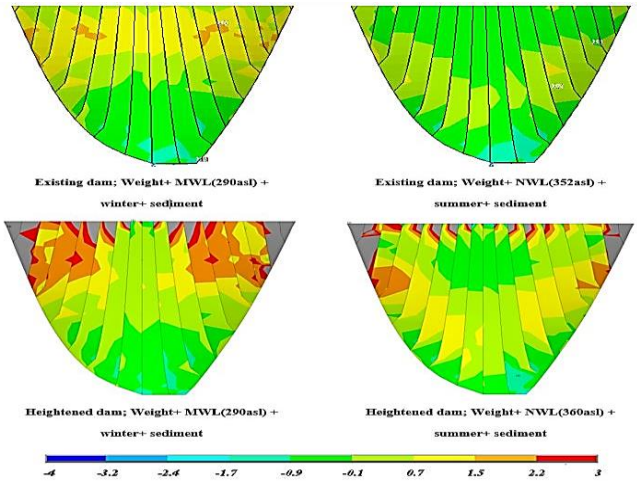

Fig. 19: Maximum principal stress distribution on the upstream face (MPa)

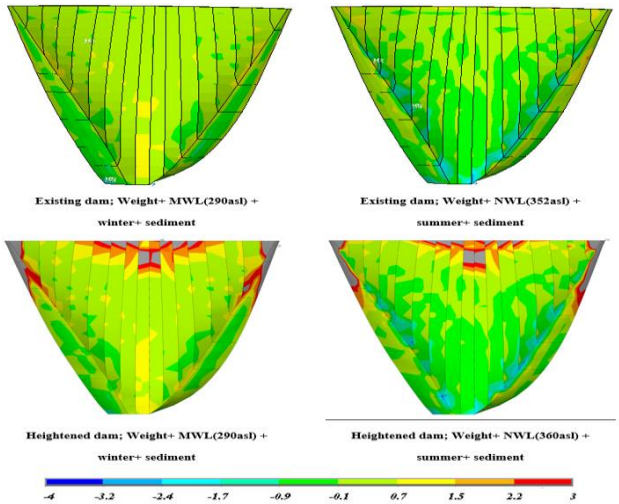

Fig. 20: Maximum principal stress distribution on the downstream face (MPa)

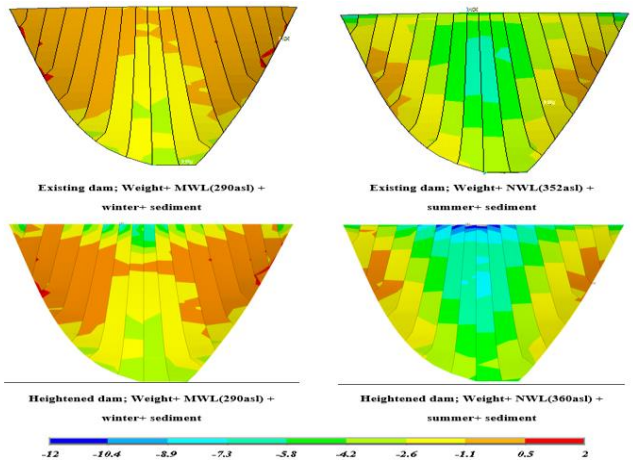

Fig. 21: Minimum principal stress distribution on the upstream face (MPa)

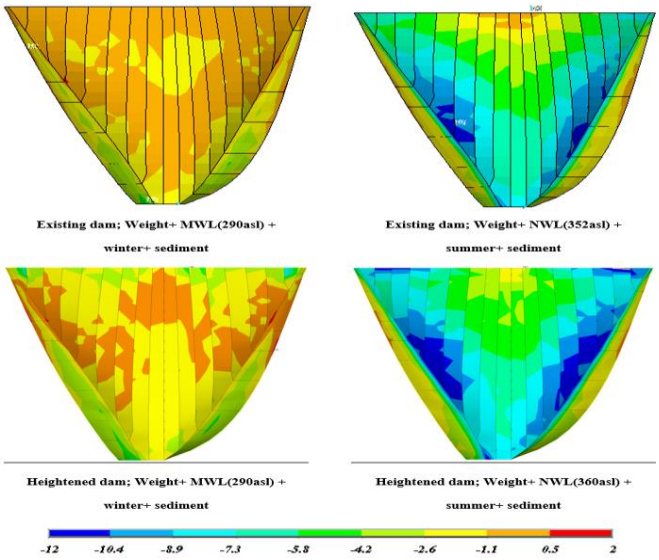

Fig. 22: Minimum principal stress distribution on the downstream face (MPa)

Based on the results of static analyses shown in Fig. **19** to Fig. 22, the stress distributions in the upper half of the dam body changes by raising the dam body. But, there is no difference between the retrofitted and initial dam's stress distribution at lower levels. Additionally, local stress concentration is observed at the new structure's interface surface and the dam body, which is expected. This trend is more evident in winter conditions. In summer conditions, local tensile stresses have effectively been removed because of the increasing compressive stress between the dam body and the new structure. Since the new structure is attached to the dam body using steel anchors, the steel anchors can absorb the predicted tensile.

5.2 Dynamic Analysis

This section reports the dynamic analyses corresponding to the summer conditions due to its critical results compared to the winter condition. Based on the static results and reports available, the initial dam's seismic performance is conducted only under MCE earthquake records. In contrast, the heightening dam seismic performance is conducted under both MCE and OBE earthquake records [22]. In the following, firstly, the seismic performance of the heightening dam is presented under OBE earthquakes. Then, the seismic performance of the existing dam and the heightened one under MCE earthquakes are compared.

5.2.1 Heightened Dam Considering Joint Nonlinearity with Linear Behavior of Mass Concrete in OBE Level

This section presents the non-concurrent envelope of tensile and compressive stresses for the heightened dam due to the OBE earthquake in summer conditions. Mass concrete of the dam body is assumed to have linear elastic behavior, but vertical joints are modeled.

Fig. **23** shows the envelope of non-concurrent maximum principal stress distribution (tensile), and Fig. **24** shows the minimum principal stress distribution (compressive). According to Fig. **23**, on the heightened dam's downstream face, tensile stresses are larger at the crest level's central blocks, whereas, on the upstream face, high tensile stresses are distributed alongside the crest. Also, on both faces, high tensile stresses are observed in the vicinity of PULVINO (Fig. **23**).

As shown in Fig. **24**, compressive stresses at the lateral blocks along the crest level on the downstream face are more substantial. But, for the upstream faces, compressive stresses are larger at the dam's central blocks at crest level, as seen in Fig. **23**. At OBE excitation, compressive stresses are not high enough to cause damage in the dam body. Additionally, in most regions of the heightened dam body, maximum principal stress distribution (tensile) is lower than the concrete tensile strength, consistent with the recommendation of guidelines [28]. It is worth noting that tensile stresses are larger than the tensile strength of mass concrete in some regions near the dam crest on both upstream and downstream faces. Such limited damage is probably due to some local stress concentrations at the junction of the initial body and new structure at the OBE level of earthquake. The anchor bars reinforced this section of the heightening structure.

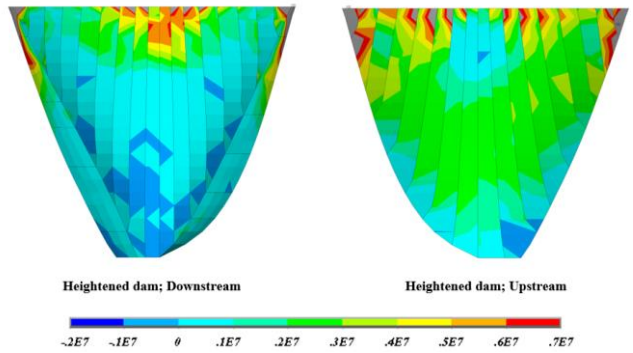

Fig. 23: Envelope of non-concurrent maximum principal stress distribution in summer under OBE record(MPa)

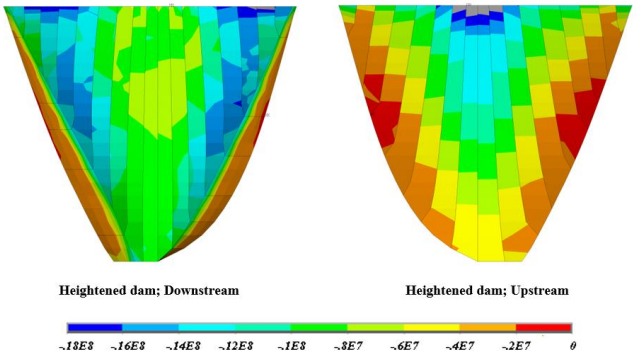

Fig. 24: Envelope of non-concurrent minimum principal stress distribution in summer under OBE record (MPa)

5.2.2 Heightened and Initial Dam Considering Joint Nonlinearity Accompanied with Linear and Nonlinear Mass Concrete in MCE Excitation

This section presents the dynamic results of the initial and heightened dam under MCE excitation corresponding to MANJIL earthquake. At first, mass concrete material behavior is assumed linear, while vertical joints are considered. Fig. **25** and Fig. **26** demonstrate the results.

Based on Fig. **25**, the initial and heightened dam have similar tensile stress distributions. On the upstream faces, at the central blocks along the crest and near abutment of the heightened dam, stress concentrations are observed with 14 MPa, which is twice the OBE earthquakes stress value. Additionally, tensile stresses at the upper half of the dam body in initial and heightened dam are larger than the tensile strength on the downstream faces. High-stress concentrations can lead to some local damage along with the crest level.

Considering the results shown in Fig. **26**, the compressive stresses envelope in the two cases of initial and heightened dams are similar. Generally, there are no significant differences between stress distributions and their values for the initial and heightened dam on the upstream and downstream faces except for some local concentration occurring at the heightened dam's crest level on the upstream face.

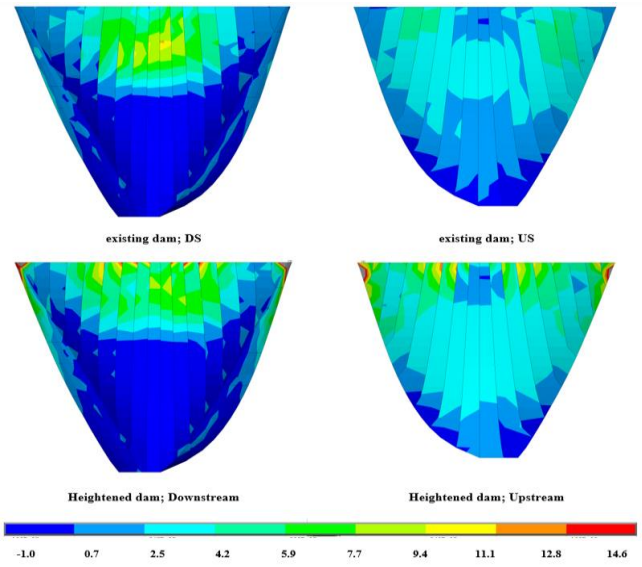

Fig. 25: Envelope of non-concurrent maximum principal stress distribution in summer and MCE (MPa)

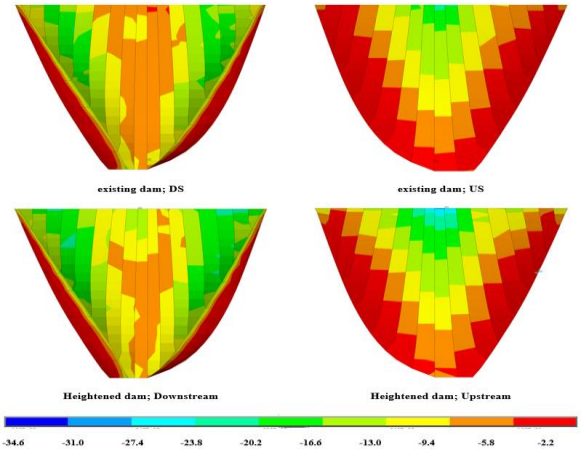

Fig. 26: Envelope of non-concurrent minimum principal stress distribution in summer and MCE (MPa)

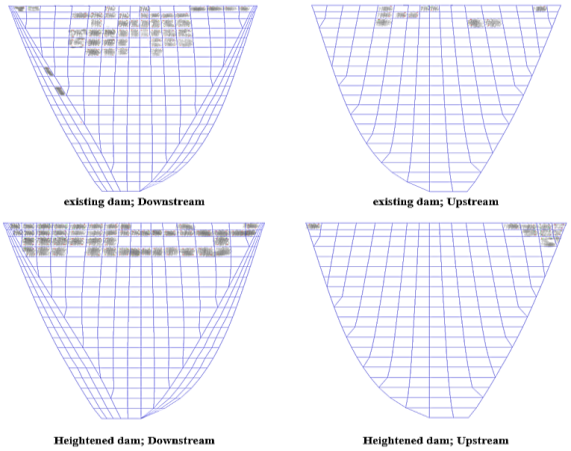

Fig. 27: Crack/crush profiles within the dam body

Assuming linear behavior for the mass concrete leads to tensile stresses beyond the tensile strength. Additionally, compressive stresses are close to the compressive strength of mass concrete (see table 5). In the following, seismic performance of DEZ dam under MCE earthquake considering non-linear behavior for the mass concrete is conducted. For this purpose, the stability of the model and crack area of the dam body is evaluated under MCE excitation. Based on the guideline "Arch Dam Design" referred to as EM-1110-2-2201, the MCE earthquake is an extreme loading condition in which significant damage is allowable but catastrophic failure of the dam body corresponding to the reservoir's sudden release should be avoided [28].

Fig. **27** shows the cracked/crushed Gaussian points in the two considered models when mass concrete has non-linear behavior in tension and compression stresses. There is no instability in the model with heightened structure. Comparing crack profiles in Fig. **27**, the cracked region's area in the heightened dam is extended along the crest. However, it can continue load-bearing after the earthquake, provided the normal water level has been raised to 360asl. Concerning the existing dam body with a massed foundation, which was evaluated as safe in MCE [30], and stress level in the heightened dam body, the heightened structure's safe performance can be concluded in summer conditions (with is the most critical load combination) in MCE.

5. Conclusion

In this study, the heightened DEZ dam's static and seismic performance is evaluated, and results are compared with the initial structure. In the static case, in both summer and winter conditions, due to the weight of the heightened structure and its structural performance at the interface surface of the new structure and the dam body, local stress concentration is observed, which is expected. However, the new structure is attached to the dam body by means of steel anchors. Values of maximum compressive and tensile stresses are far more than mass concrete strength.

In the dynamic condition under OBE excitation, regions with high concentrated compressive stresses on the upstream face are limited in the central blocks and at the crest level on the downstream face, due to attaching the new structure. Some structural damages in OBE are expected based on the observed high tensile stresses in the heightened dam body.

In the dynamic conditions of MCE, increasing normal water levels has no significant effect on the tensile stress distribution on both faces of the dam. However, high-stress concentrations in the dam body's junction and the new structure occur and can lead to some local failure at these locations along with the crest level. The compressive stress envelope in the heightened dam is similar to that in the existing one. However, some local stress concentrations in the central region at the crest level are observed. The cracked region in the heightened dam is extended along the crest. Based on the results, some extensive damage is expected in lateral blocks at the crest level. Nevertheless, this damage doesn't lead to the sudden release of the reservoir. Based on the above numerical results, the safe performance of the heightened structure can be concluded in MCE

References

[1] Feuz, Bernard. "Raising of the Mauvoisin Dam." *Structural Engineering International* 4.2 (1994): 103-104.

[2] WAPDA, Pakistan. "Mangla dam raising project." *Feasibility Study Report* 1 (2001).

[3] Keller, T. O., et al. "Raising San Vicente Dam: Why and How." *HYDRO REVIEW* 26.4 (2007): 26.

[4] Boroujeni, H. Samadi. "Sediment Management in Hydropower Dam (Case Study–Dez Dam Project)." *Hydropower-Practice and Application*. IntechOpen, 2012.

[5] Borotijeni, H. S. "Investigation un Bulk Density of Deposited Sediments in Dez Reservoir." *Trends in Applied Sciences Research* 4.3 (2009): I4S-I57.

[6] Tolouie, E., J. R. West, and J. Billam. "Sedimentation and desiltation in the Sefid-Rud reservoir, Iran." *Geomorphology and sedimentology of lakes and reservoirs. J. Wiley & Sons, England, Chapt* 9 (1993): 125-138.

[7] Graf, William L., et al. "Sedimentation and sustainability of western American reservoirs." Water Resources Research 46.12 (2010).

[8] Issa, Issa E. *Siltation and sedimentation problem in Mosul reservoir dam*. Diss. Luleå tekniska universitet, 2013.

[9] Kondolf, G. Mathias, et al. "Sustainable sediment management in reservoirs and regulated rivers: Experiences from five continents." *Earth's Future* 2.5 (2014): 256-280.

[10] Tang, Xianqiang, Min Wu, and Rui Li. "Distribution, sedimentation, and bioavailability of particulate phosphorus in the mainstream of the Three Gorges Reservoir." *Water research* 140 (2018): 44-55.

[11] Huang, Yifan, Jinsheng Wang, and Mei Yang. "Unexpected sedimentation patterns upstream and downstream of the Three Gorges Reservoir: Future risks." *International journal of sediment research* (2018).

[12] Guertault, L., and G. A. Fox. "Impact of Data Availability and Resolution on Long-Term Sedimentation Estimates in a Storage Reservoir." *Journal of Hydrologic Engineering* 23.10 (2018): 05018019.

[13] Tadesse, Abebe, and Wenhong Dai. "Prediction of sedimentation in reservoirs by combining catchment based model and stream based model with limited data." *International journal of sediment research* 34.1 (2019): 27-37.

[14] Samadi-Boroujeni, H., A. H. Haghiabi, and E. Ardalan. "Determination of appropriate hydraulic conditions to decrease the negative impacts of Dez dam flushing operation on the." *International Journal of Water Resources and Environmental Engineering* 2.2147483648 (2010): 001-008.

[15] Ghorbani, Mortaza Ali, Majid Pasbani Khiavi, and Parya Ahmadi. "Investigation of Nonlinear Behavior of Concrete on Seismic Performance of an Arch Dam Using Finite Element Method." *Civil Engineering Journal* 2.6 (2016): 295-305.

[16] Ghaemian, Mohsen, Ali Noorzad, and Hamid Mohammadnezhad. "Assessment of foundation mass and earthquake input mechanism effect on dam–reservoir–foundation system response." *International Journal of Civil Engineering* 17.4 (2019): 473-480.

[17] Mostafaei, Hasan, Morteza Sohrabi Gilani, and Mohsen Ghaemian. "A Comparative Study between Pseudo-static and Dynamic Analyses on Rock Wedge Stability of an Arch Dam." *Civil Engineering Journal* 4.1 (2018): 179-187.

[18] Mostafaei, Hasan, Morteza Sohrabi Gilani, and Mohsen Ghaemian. "Stability analysis of arch dam abutments due to seismic loading." *Scientia Iranica* 24.2 (2017): 467-475.

[19] Chen, Deng-Hong, et al. "Seismic performance and failure modes of the Jin'anqiao concrete gravity dam based on incremental dynamic analysis." *Engineering Failure Analysis*100 (2019): 227-244.

[20] Lin, Peng, et al. "Horizontal cracking and crack repair analysis of a super high arch dam based on fracture toughness." *Engineering Failure Analysis* 97 (2019): 72-90.

[21] Behan-sad Engineering and consulting Co., Seismic hazard analysis of DEZ dam, 2009, Tehran, Iran.

[22] Hariri-Ardebili, M. A., H. Mirzabozorg, and M. Ghaemian. "Pulvino and peripheral joint effects on static and seismic safety of concrete arch dams." *Scientia Iranica* 20.6 (2013): 1579-1594.

[23] Water and power ministry, Design and analysis of DEZ dam, 1963, Tehran, Iran.

[24] Hariri-Ardebili, M. A., and H. Mirzabozorg. "Feasibility study of Dez arch dam heightening based on non-linear numerical analysis of existing dam." *Archives of Civil Engineering* 59.1 (2013): 21-49.

[25] Willam, K. J., and E. P. Warnke. "Constitutive Model for the Triaxial Behavior of Concrete, IABSE Report Vol. 19, 1974." *Colloquium on "Concrete Structures Subjected to Triaxial Stress", ISMES Bergamo*. 1974.

[26] Federal Energy Regulatory Commission. "Engineering guidelines for the evaluation of hydropower projects. Chapter 11-Arch Dams." *Washington DC* 20426 (1999): 11-18.

[27] Lysmer, John, and Roger L. Kuhlemeyer. "Finite dynamic model for infinite media." *Journal of the Engineering Mechanics Division* 95.4 (1969): 859-878.

[28] USACE. 1994. *Arch dam design, Engineering Manual EM 1110-2-2201*. US Army Corps of Engineers, Washington DC.

29- Hall, John F. "Efficient non-linear seismic analysis of arch dams." *Earthquake engineering & structural dynamics* 27.12 (1998): 1425-1444.

[29] Behan-sad Engineering and consulting Co., Seismic hazard analysis of DEZ dam, 2009, Tehran, Iran.